Solar Physics
DOI: 10.1007/•••••-•••-•••-••••-•

Active-Region Twist Derived from Magnetic Tongues and Linear Force-Free Extrapolations

Mariano Poisson[1] · Marcelo López Fuentes[1] · Cristina H. Mandrini[1,2] · Pascal Démoulin[3]

Abstract The main aim of this study is to compare the amount of twist present in emerging active regions (ARs) from photospheric and coronal data. We use linear force-free field models of the observed coronal structure of ARs to determine the global twist. The coronal twist is derived, on one hand, from the force-free parameter $[\alpha]$ of the model and, on the other, from the computed coronal magnetic helicity normalized by the magnetic flux squared. We compare our results, for the same set of ARs, with those of Poisson *et al.* (2015, *Solar Phys.* **290**, 727), in which the twist was estimated using the "magnetic tongues" observed in line-of-sight magnetograms during AR emergence. We corroborate the agreement between the photospheric and coronal twist-sign and the presence of magnetic tongues as an early proxy of the AR non-potentiality. We find a globally linear relationship between the coronal twist and the one previously deduced for the emerging AR flux rope at the photospheric level. The coronal twist value is typically much lower, by a factor of six, than the one deduced for the emerging flux rope. We interpret this result as due to the partial emergence of the flux rope that forms the region.

Keywords: Active Regions, Magnetic Fields – Active Regions, Structure – Corona, Models – Helicity, Magnetic

✉ M.López Fuentes
lopezf@iafe.uba.ar

[1] Instituto de Astronomía y Física del Espacio (IAFE), CONICET-UBA, Buenos Aires, Argentina

[2] Facultad de Ciencias Exactas y Naturales (FCEN), UBA, Buenos Aires, Argentina

[3] Observatoire de Paris, LESIA, UMR 8109 (CNRS), F-92195 Meudon Principal Cedex, France

1. Introduction

The magnetic-field generation and amplification in the solar interior, *i.e.* the solar dynamo, is thought to be responsible for the production of non-potential or twisted flux-tubes (*i.e.* flux ropes, see, *e.g.*, Fan, 2009). These concentrated magnetic fields carry an important amount of magnetic helicity from the convective zone to the solar atmosphere, through their emergence at the photospheric level as active regions (ARs). The presence of magnetic helicity in the Sun is evident from observed features such as sunspot whorls, the spatial organization of fibrils and feet or barbs of filaments, and the sigmoidal distribution of coronal loops in ARs, among others (Démoulin and Pariat, 2009). The origin of the helicity, due to the action of turbulent helical motions in the solar interior, is strongly suggested by the hemispherical chirality rule satisfied, in general, by these features (Pevtsov *et al.*, 2014).

From the theoretical side, the presence of twist in emerging magnetic-flux tubes is a necessary condition for their ability to survive the transit across the convective zone (Emonet and Moreno-Insertis, 1998; Fan, 2001). More recently, numerical studies have found that the twist also plays a role in the process by which the flux tubes cross the interface between the solar interior and the photosphere (Hood, Archontis, and MacTaggart, 2012). Detailed observations of the first stages of emergence at the photosphere, while broadly confirming these theoretical and numerical results, also show a complex process where the main flux rope is split into many thin ones at the photospheric level before reorganizing to a more coherent magnetic configuration in the corona (Pariat *et al.*, 2004; Valori *et al.*, 2012; Vargas Domínguez, van Driel-Gesztelyi, and Bellot Rubio, 2012).

The helicity in twisted emerging structures is related to the presence of electric currents and, therefore, to the free magnetic-energy content of these structures. That is why ARs with a highly twisted coronal structure are prone to produce active phenomena, such as flares and coronal mass ejections (CMEs), in larger numbers and with higher energies (see, *e.g.*, Tziotziou, Georgoulis, and Raouafi, 2012; Szajko *et al.*, 2013). Much of the magnetic helicity produced in the Sun is ultimately removed by the ejection of magnetic structures into the interplanetary medium in the form of CMEs (Mandrini *et al.*, 2004; Démoulin and Pariat, 2009).

In a recent article (Poisson *et al.*, 2015), we thoroughly studied a particular photospheric feature associated with the presence of twist in ARs: the so-called "magnetic tongues" (or tails), which appear as deformations of the main polarities in photospheric magnetograms of emerging bipolar ARs. Assuming that ARs are produced by the emergence of Ω-shaped magnetic-flux tubes, the presence of twist implies that the field lines wrap around the main axis of the tube producing a non-null azimuthal component. The projection of this azimuthal component on the line-of-sight (LOS) direction is the cause of the observed magnetic polarity deformations or "tongues". In Poisson *et al.* (2015), we defined and studied a series of parameters to characterize magnetic tongues during the emergence of bipolar ARs. In particular, we developed a procedure to study the evolution of the angle that the polarity invertion line (PIL) forms with the direction orthogonal to the main axis of the AR bipole (*i.e.* the line that joins the

barycenters of the positive and negative polarities as defined by López Fuentes *et al.*, 2000). This so-called tongue angle has a zero value for an untwisted flux tube and grows monotonically as a function of the flux-tube twist. The sign of the tongue angle was shown to be consistent with the helicity sign derived from photospheric helicity flux injection (computed from magnetogram time series), from sheared coronal loops, from sigmoids, from flare ribbons, and/or from the associated magnetic cloud observed *in situ* at 1 AU (Luoni *et al.*, 2011).

Although the transfer of magnetic helicity from the convective zone into the corona can be complex, since magnetic helicity is an almost-conserved quantity in resistive plasmas with a high magnetic Reynolds number (Berger, 1984), we expect that, at least, its sign at the photosphere should be conserved at the coronal level. Previous works have addressed this issue by comparing the sign of the force-free parameter $[\alpha]$ of the photospheric currents computed from vector magnetograms to the sign derived by fitting a linear force-free model to the observed chromospheric fibrils and coronal loops (Burnette, Canfield, and Pevtsov, 2004; Gosain, Démoulin, and López Fuentes, 2014).

In this article, we focus again on the analysis of the twist of the same set of ARs studied by Poisson *et al.* (2015). Our motivation is to go one step farther and to quantitatively analyze the relation between the twist determined at the photospheric level to that inferred from coronal magnetic-field modeling. A major assumption of our analysis is that an AR results from the emergence of a flux rope (see Poisson *et al.*, 2015).

In Section 2 we describe the data used in this article. In Section 3 we provide a description of the method followed to model the coronal structure of the observed ARs. In Section 4 we relate the force-free parameter derived from the coronal model with two different definitions of the "number of turns" that we associate with the coronal twist. In Section 5 we present and discuss our results and, finally, we compare them with the number of turns derived by Poisson *et al.* (2015) using magnetic tongues. We conclude in Section 6.

2. Data Description

We use data from the *Michelson Doppler Imager* (MDI: Scherrer *et al.*, 1995) and the *EUV Imaging Telescope* (EIT: Delaboudinière *et al.*, 1995), both onboard the *Solar and Heliospheric Observatory* (SOHO) for most of the studied ARs. For two of them, we use data from the *Helioseismic and Magnetic Imager* (HMI: Scherrer *et al.*, 2012) and the *Atmospheric Imaging Assembly* (AIA: Lemen *et al.*, 2012). MDI and HMI provide LOS magnetograms, which are used to extrapolate the photospheric magnetic field to the corona following the procedure described in Section 3. EIT and AIA images in the 171, 195, and 284 Å channels that are nearly cotemporal with the magnetogram are used to compare the observed AR coronal structure with the modeled field lines to find the best-fit parameters. The set of ARs in this article is the same used by Poisson *et al.* (2015, see Table 1). The first and second columns of Table 1 show the NOAA numbers and the observation dates and times of the analyzed ARs. These dates have been chosen following the criteria discussed in Section 3. The data are processed and

coaligned using the tools available in the Solar Software package. As explained by Poisson *et al.* (2015), the LOS component of the magnetic field provided by the magnetograms is projected onto the local vertical component (the normal to the photosphere).

3. Linear Force-Free Field Model

In this section we describe the method followed to determine the α-parameter that will be used to quantify the twist of the ARs. The procedure consists of the linear force-free extrapolation into the corona of the photospheric magnetograms. The computation is based on a fast Fourier transform (FFT) of the equation

$$\nabla \times \boldsymbol{B} = \alpha \boldsymbol{B}, \tag{1}$$

where $\boldsymbol{B}$ is the magnetic field and α is a constant (Alissandrakis, 1981). Using the magnetograms as photospheric boundary condition, the extrapolation code provides, for a given value of the α-parameter, the three components of the magnetic field on each mesh point of a gridded computational box that corresponds to the coronal volume occupied by the AR. Using models with different values of α we integrate and trace sets of field lines that are compared with coronal loops observed with EIT or AIA. The value of α that best matches the observed coronal loops is used to quantify the AR twist (see Section 4). The fitting procedure itself consists in selecting sets of points along the observed loops. The best model is the one that minimizes the distance between the modeled field lines and the selected loop points. A detailed description of the procedure is provided by Green *et al.* (2002) (see also López Fuentes, Klimchuk, and Démoulin, 2006; Gosain, Démoulin, and López Fuentes, 2014). Since for AR coronal fields the force-free Equation (1) is non-linear (*i.e.* α is not a constant) the best α-value found here is a compromise to best fit on average the different observed loops. We think that for the main objective of the present work, which is to quantify the global twist of an AR, the linear approximation and then obtaining a single representative α value is appropriate. It is worth reminding that the ARs analyzed here belong to the set used by Poisson *et al.* (2015). The main objective in that article was to develop a method to characterize the effect of the magnetic tongues on photospheric magnetograms using the direction of the PIL. That is why the selected ARs are bipolar, because their relative simplicity facilitates the determination of the PIL. The fact that the ARs are not complex further justifies the use of a constant α. In very complex ARs this approximation would be more difficult to sustain.

The computation code uses as a boundary condition the component of the magnetic field that is normal to the photosphere (see Section 2). The procedure for obtaining the normal component is less reliable when the AR is farther from the center of the solar disk, since in that case the unknown contribution of the transverse components of the field becomes increasingly larger. Therefore, the closer the AR is to the center of the disk the better the approximation of projecting the field in the local vertical direction is. Our first criterion for the

choice of the observation date for the extrapolations is, then, that the AR must be as close to central meridian passage (CMP) as possible in the available data set.

The second criterion is based on the amount of emerged magnetic flux of the AR. It is expected that the twist be much better defined around the time of maximum photospheric flux. Before the maximum magnetic flux is reached, the AR is still emerging and its twist has not been entirely injected into the corona. Eruptive flaring can remove twist during the full AR lifetime, while after the maximum flux, due in part to the dispersion of the field, the observed structure relaxes. Both effects result in an increasingly less important twist. However, all effects taken into account, the closer the analysis is to the date of maximum magnetic flux, the larger is the expected signal for the twist determination.

The compromise between the two criteria discussed above, implies that for the analysis we should choose the date of maximum magnetic flux whenever the AR was not farther than 40 heliographic degrees from the CMP. If at the date of maximum flux the AR was outside that spatial range, we chose a date closer to the maximum flux within that range. In any case, the magnetic flux of the AR at the date of the analysis cannot be below 70 % of the maximum flux. All of the ARs in Table 1 fulfil these criteria at the chosen dates.

In Figures 1 – 3 we show examples of modeled coronal structures for some of the ARs listed in Table 1. Each figure presents two ARs (upper and lower panels, respectively), so that for each AR the left panel corresponds to the EUV image and the right panel shows the modeled structure represented by field lines (in red) integrated using the best-fitting magnetic model. Figure 1 shows two examples of ARs with negative twist: AR 10440 (panels a and b) and AR 10569 (panels c and d). Figure 2 corresponds to ARs with positive twist: AR 10900 (panels a and b) and AR 10987 (panels c and d). In all cases, notice how the shape of the field lines and observed loops determines the twist sign. Finally, in Figure 3, the upper panels (a and b) correspond to AR 10664, an AR whose magnetic structure is very close to potential, and the lower panels (c and d) show an example of an AR (11141) observed with SDO/AIA.

Following the procedure and the criteria described in this section, we determine the best values of α for all of the analyzed ARs listed in Table 1. It is worth mentioning that not all of the 41 ARs studied by Poisson *et al.* (2015) have been considered in the present analysis. ARs NOAA 10727, 10828, and 11005 are not included either because EIT data are not available for the dates required by our selection criteria or because the visibility of the coronal loops is not good enough to allow us to determine a reliable best value of α.

4. The Twist as the Number of Turns

In Poisson *et al.* (2015), we used as a measure of the AR twist the number of turns of a hypothetical emerging magnetic flux-tube. Here, we follow the same concept but using linear force-free field (LFFF) models. In the next subsections, we explore different ways to establish a relation between the α-parameter and the twist defined as the number of turns.

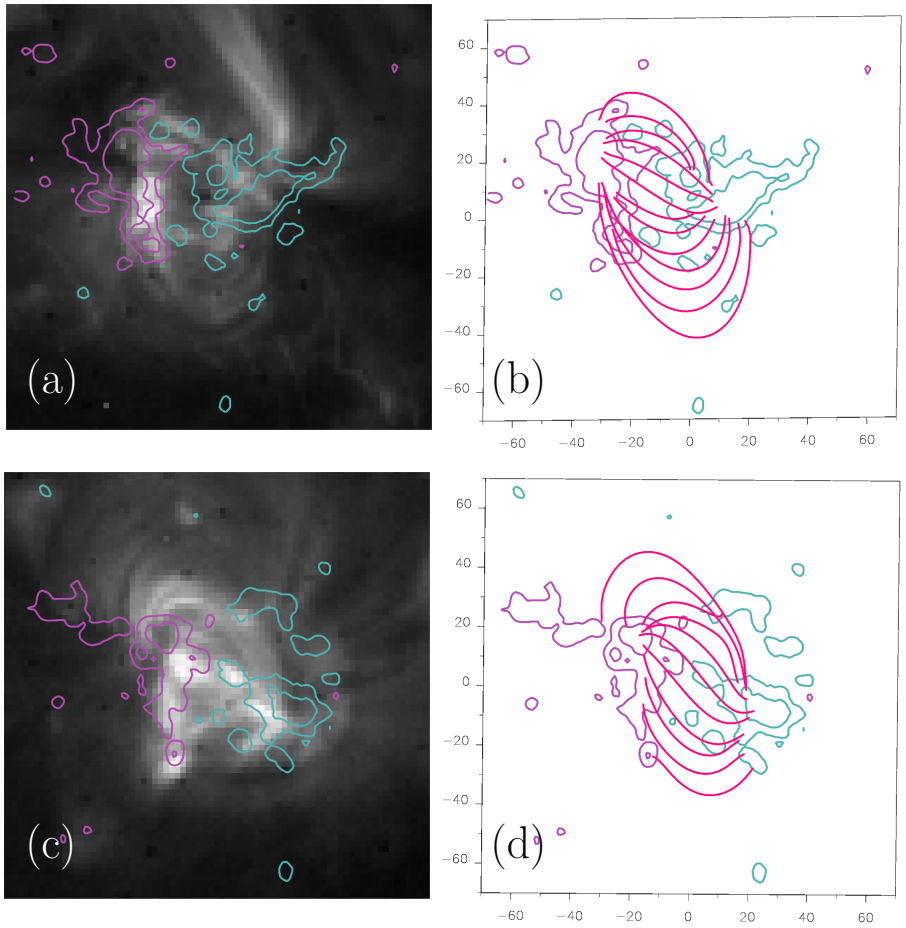

Figure 1. Examples of ARs with negative twist. (a) SOHO/EIT image of AR 10440 in the 195 Å channel, obtained on 22 August 2003 at 19:11 UT. (b) Best-fitting model corresponding to $\alpha = -1.9 \times 10^{-2}$ Mm^{-1}. (c) SOHO/EIT image of AR 10569 in 195 Å, obtained on 07 March 2004 at 08:03 UT. (d) Model corresponding to $\alpha = -2.4 \times 10^{-2}$ Mm^{-1}. In all panels the colored contours correspond to photospheric magnetic-field values of 100 G and 500 G. Magenta-continuous lines indicate positive field and green lines correspond to negative field. In panels b and d sets of computed field lines are shown in red. Coordinate units are Mm.

4.1. Magnetic Helicity from LFFF Extrapolations

The magnetic helicity [H] is directly computed from the LFFF model (Berger, 1985). This has been explored by Démoulin *et al.* (2002) and Green *et al.* (2002). In the Appendix of the latter article we analyzed the dependence of the magnetic helicity as a function of α and the contribution of the components of the different Fourier modes. The helicity expression presented there (see their Equation (10)) corresponds to the relative helicity with respect to the potential solution of the

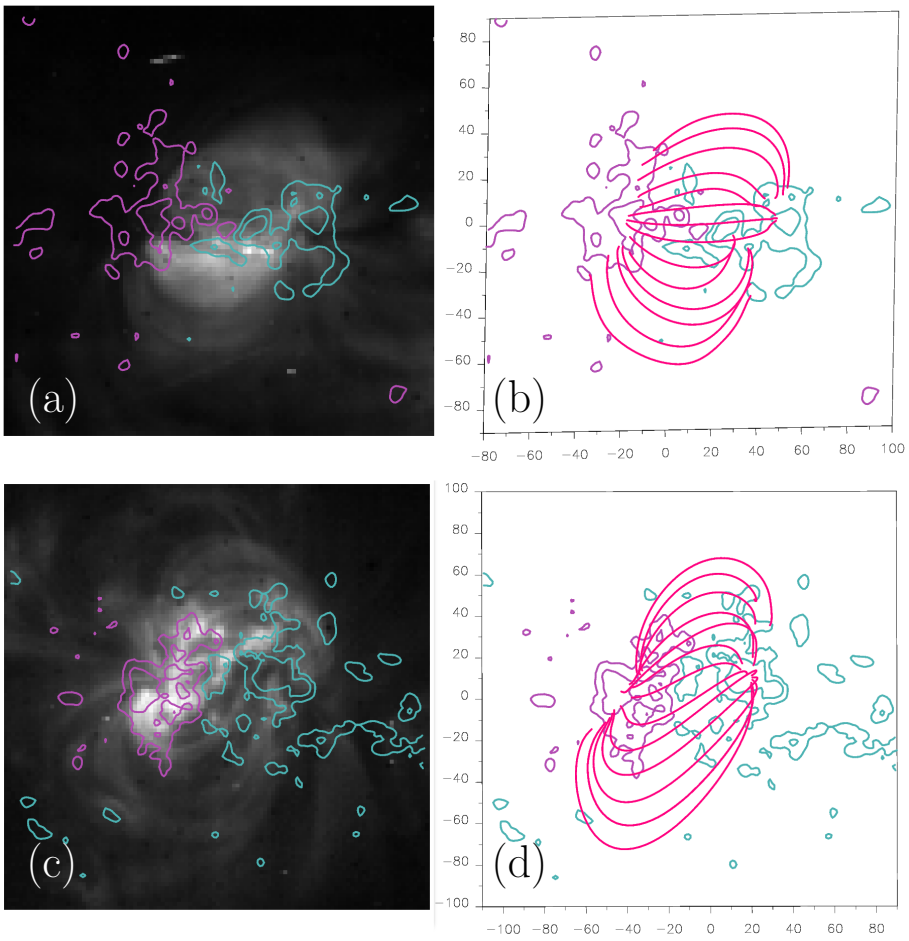

Figure 2. Examples of ARs with positive twist. (a) SOHO/EIT image of AR 10900 in the 284 Å channel, obtained on 19 July 2007 at 01:36 UT. (b) Best-fitting model corresponding to $\alpha = 6.3\times10^{-3}$ Mm^{-1}. (c) SOHO/EIT image of AR 10987 in 195 Å, obtained on 27 March 2008 at 12:47 UT. (d) Model corresponding to $\alpha = 1.6\times10^{-2}$ Mm^{-1}. In all panels colored contours correspond to photospheric magnetic-field levels of 100 G and 500 G. Magenta-continuous lines indicate positive field and green lines correspond to negative field. In panels b and d sets of field lines are shown in red. Coordinate units are Mm.

field with the same photospheric boundary (vertical component of the magnetic field). The use of the relative helicity avoids the known gauge-dependence problem when computing H (see Berger, 1984). Démoulin *et al.* (2002) and Green *et al.* (2002) introduced a linearized form of the helicity expression (see, *e.g.*, Equation (11) in the latter article) in order to avoid the unrealistic growth of H as it diverges when α approaches its resonant values. We remark that all of the best values of α in the LFFF models of this article stay below the resonant

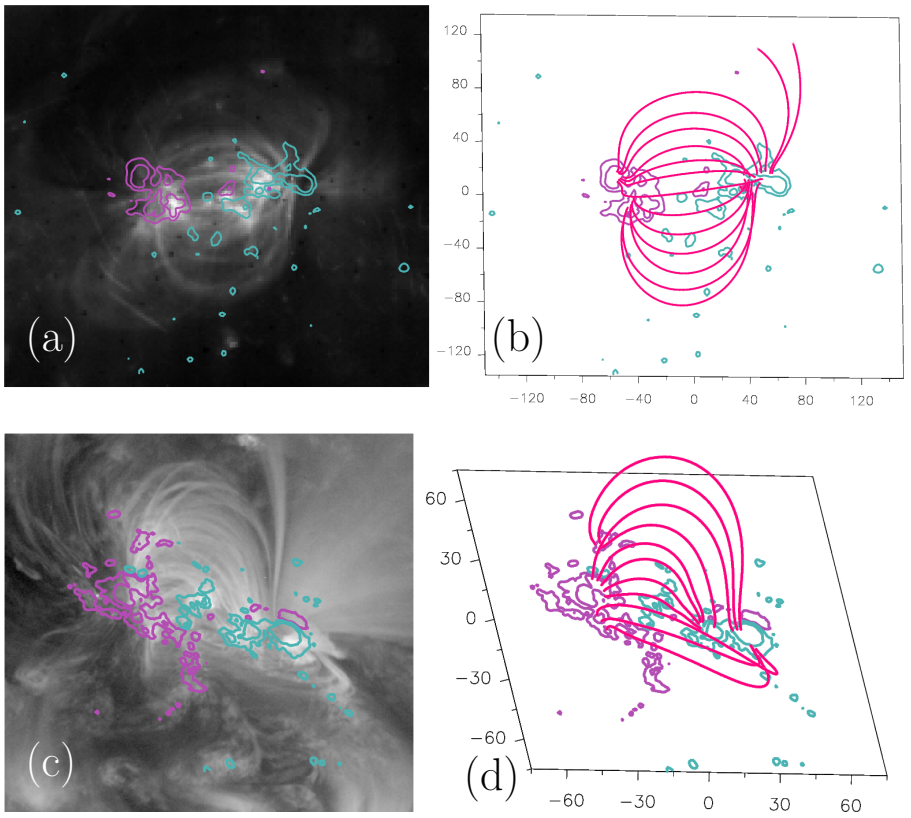

Figure 3. (a) SOHO/EIT image in the 195 Å channel of AR 10664, obtained on 23 August 2004 at 11:11 UT. This is an AR with an observed coronal structure very close to potential. (b) Best-fitting model corresponding to $\alpha = 3.1 \times 10^{-3}$ Mm^{-1}. (c) SDO/AIA image of AR 11141 in the 171 Å band, obtained on 01 January 2011 at 19:00 UT. (d) Model corresponding to $\alpha = -9.4 \times 10^{-3}$ Mm^{-1}. In all panels colored contours correspond to photospheric magnetic-field levels of 100 G and 500 G. Magenta-continuous lines indicate positive field and green lines correspond to negative field. In panels b and d sets of field lines are shown in red. Coordinate units are Mm.

values. A typographical error (a factor 2) was present in Equation (11) of Green *et al.* (2002); this was corrected in Mandrini *et al.* (2005). The correct expression is:

$$H = \alpha \sum_{n_x=0}^{N_x} \sum_{n_y=0}^{N_y} \frac{|\widetilde{B}^2_{n_x,n_y}|}{(k_x^2 + k_y^2)^{3/2}}\,, \tag{2}$$

where the mode $n_x = n_y = 0$ (uniform field) has no contribution ($\widetilde{B}_{0,0}$ is set to zero), $\widetilde{B}_{n_x,n_y}$ is the Fourier amplitude of the harmonic (n_x, n_y), $k_x = 2\pi n_x/L$,

$k_y = 2\pi n_y/L$, L being the horizontal extension of the computational box. In this work, we use this linearized form to compute H (Table 1).

The magnetic helicity of a uniformly twisted flux tube with N turns and an axial magnetic flux Φ is $N\Phi^2$ (*e.g.* Berger, 1999). This expression neglects the contribution of the writhe, which is the helicity associated to the flux-tube deformation as a whole. Then, we define a number of turns associated to the helicity computed from the LFFF model as:

$$N_{\rm H} = H/\Phi^2. \tag{3}$$

We use the notation $N_{\rm H}$ to differentiate this definition of the number of turns from the one given by Poisson *et al.* (2015) [$N_{\rm t}$]. Table 1 shows the values of $N_{\rm H}$ computed using Equation (3) from the helicities listed in the corresponding column.

The magnetic flux [Φ] used corresponds to the unsigned mean of the positive and negative flux of the AR computed as follows. We selected rectangular boxes from the full-disk magnetograms, that we call observational boxes, with similar relative sizes for all ARs. In all cases, we computed Φ considering only the flux belonging exclusively to the AR, so the observational boxes were set to have the minimum possible size that contains the relevant flux. Since the observed magnetic flux of the positive and negative polarities of an AR are in general unbalanced, an error is expected in the computed mean flux. To characterize the typical flux imbalance of the ARs in our set, let us define the relative imbalance as the absolute value of the difference between the unsigned positive and negative fluxes divided by the computed mean flux ($|\Phi_+ - |\Phi_-||/\Phi$). If we consider the relative error in the flux as one half of the relative flux imbalance ($\Delta\Phi = |\Phi_+ - |\Phi_-||/2$), then the mean relative error of the flux for the 38 ARs in our set is approximately 0.05; 26 ARs are below that value and only five are above 0.1. If we consider only the effect of Φ (neglecting the effect of H) on the error of $N_{\rm H}$, a simple propagation from Equation (3) indicates that the relative error in $N_{\rm H}$ is equal to twice the relative error in Φ. Therefore, as a rough estimation, the mean relative error in $N_{\rm H}$ due to the flux imbalance, for the ARs in our set is approximately 0.1.

It is important to indicate here that H is calculated in a computational box that is larger than that used to compute Φ. This is because the periodic boundary conditions of the FFT method require imposing a low-field area around the observed magnetogram to avoid aliasing effects (Alissandrakis, 1981). Therefore, the computation of H, which is done for the full computational box, overestimates the actual magnetic-helicity content of the AR. Moreover, since in a LFFF model the largest structures are the most important contributors to the helicity, all long field lines artificially included in this box further increase the helicity overestimation. In Section 5 we discuss the implications of this approximation for the robustness of $N_{\rm H}$ as a proxy of the ARs twist.

4.2. Linear Force-Free Flux-Rope: the Lundquist Solution

In this section we discuss how the α-parameter from the LFFF model can be related to the concept of twist in a simple configuration, such as a straight

cylindrical flux rope. Our aim is to provide a more geometrical interpretation of the number of turns and to compare this approach with the results computed using Equation (3).

We use the classical solution for the magnetic field of a cylindrical force-free flux rope with constant α, known as the Lundquist solution (see, *e.g.*, Sturrock, 1994):

$$\boldsymbol{B} = (B_r, B_\theta, B_z) = B_0(0, J_1(\alpha r), J_0(\alpha r)), \tag{4}$$

where B_0 is the magnetic-field intensity at the axis of the rope, and J_0 and J_1 are the Bessel functions of order 0 and 1. Given the radial and azimuthal components of the field, the twist (expressed as an angle *per* unit length) of the flux rope is:

$$b(r) = \frac{\mathrm{d}\theta}{\mathrm{d}z} = \frac{1}{r}\frac{B_\theta}{B_z}. \tag{5}$$

Then, for the Lundquist flux rope:

$$b(r) = \frac{J_1(\alpha r)}{r J_0(\alpha r)} \tag{6}$$

The above equation diverges as J_0 tends to its first root ($\alpha r \approx 2.4$), but for smaller r values ($\alpha r \lesssim 1$), it can be shown that $b(r) \approx \alpha/2$ (see also Longcope and Welsch, 2000). Since $b(r)$ is the angle in radians *per* unit length, the number of turns in a rope of length L is

$$N_\alpha = \frac{bL}{2\pi} \approx \frac{\alpha L}{4\pi}. \tag{7}$$

Here we use the subscript α to distiguish this value from N_H in Equation (3).

The above computation considers the simple case of a straight flux rope. However, the emerging flux-ropes that form ARs are thought to have a toroidal shape (similar to the Greek letter Ω). Computing the twist in the case of a bent Ω flux-rope would be more complicated, because in that case the field lines would be deformed by the redistribution of the magnetic tension and the torques associated to the flux-rope bending. Nevertheless, in order to provide a simple relation between the twist and α in the framework of the present analysis, we think that the above expression is enough. As a rough approximation, one can simply geometrically bend the above straight flux tube to half a torus. So, for an ideal bipolar AR with its main polarities separated by a distance D, the length of half the torus is $\pi D/2$. Then,

$$N_\alpha = \frac{\alpha D}{8}. \tag{8}$$

The separation of the polarities $[D]$ is computed as the distance between the barycenters of the positive and negative polarities (see López Fuentes *et al.*, 2000) for values of the radial-field component above 10 G. The previous expression can be compared with a similar result by Pevtsov, Maleev, and Longcope (2003, see, in particular, their Equation (1)) in which 8 is replaced by 2π. For comparison

with the previous result, in Appendix A we analyze the case of a flux tube with constant twist, the so-called Gold–Hoyle flux-tube solution. We show that, although for the Gold–Hoyle model α is a function of the position across the flux-tube radius, under reasonable approximations Equation (8) still holds. In the last column of Table 1 we list the values of N_α computed from Equation (8) for the set of analyzed ARs.

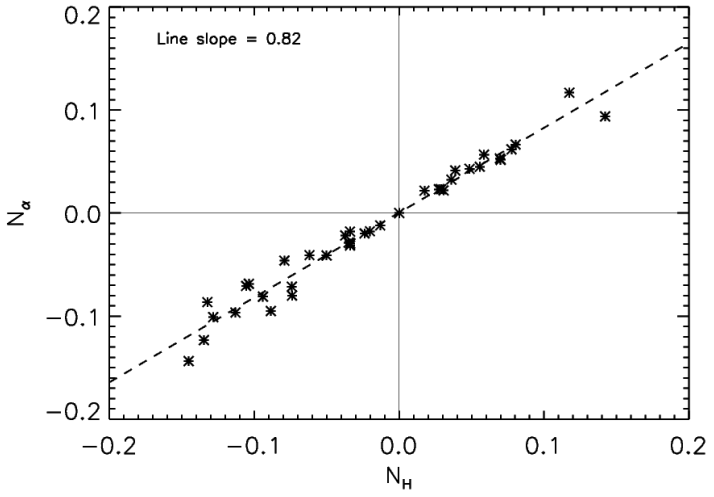

Figure 4. Number of turns [N_α], obtained from Equation (8), *vs.* N_H, obtained from Equation (3), for the ARs listed in Table 1. The dashed line corresponds to a linear regression of the data.

5. ARs Twist from Magnetic Tongues and LFFF Models

In this section we analyze our results and compare them with those obtained in Poisson *et al.* (2015). Table 1 lists the ARs ordered by NOAA number, the observation dates and times of the magnetograms used as boundary conditions of the LFFF models, the AR positions in heliographic coordinates, the best α values and the relative helicities [H] computed from the models, the unsigned magnetic fluxes of the ARs [Φ], the distances between the barycenters of the positive and negative polarities [D], the numbers of turns obtained from the magnetic tongues [N_t], the numbers of turns computed from H using Equation (3), and the numbers of turns computed directly from α using Equation (8). The helicity, magnetic-flux, and distance values in the list are consistent with those obtained for ARs in other articles (López Fuentes *et al.*, 2003; Holder *et al.*, 2004; Yang, Zhang, and Büchner, 2009, see also references in Démoulin and Pariat, 2009 and Pevtsov *et al.*, 2014).

In Figure 4 we plot N_α *vs.* N_H. The clear linear relation between the two parameters shows that the approximations considered to obtain Equation (8)

Table 1. List of studied ARs and the corresponding parameters used in our analysis (see Section 5 for a detailed description of the table contents).

AR Numb.	Obs. Date [UT]	AR Hel. Position	α [10^{-2} Mm^{-1}]	H [10^{42} Mx^2]	Φ [10^{22} Mx]	D [Mm]	N_t	N_H	N_α
10268	SOL2003-01-23T17:38	W02 N13	-1.88	-0.52	0.32	17.4	-0.83	-0.05	-0.04
10274	SOL2003-02-04T01:35	W10 S07	1.26	1.03	0.38	32.9	0.57	0.07	0.05
10311	SOL2003-03-13T06:27	W00 S12	-0.31	-0.94	0.68	45.0	-0.18	-0.02	-0.02
10319	SOL2003-03-29T06:24	W20 N12	0.00	0.00	1.92	82.9	-0.09	0.00	0.00
10323	SOL2003-03-31T19:15	W28 S08	0.63	26.7	1.86	78.7	0.24	0.08	0.06
10344	SOL2003-04-27T19:12	E01 N16	0.63	8.24	1.46	52.7	0.11	0.04	0.04
10349	SOL2003-05-01T06:27	W00 S15	-0.13	-12.8	3.13	76.3	-0.13	-0.01	-0.01
10381	SOL2003-06-13T12:46	E02 S18	-1.88	-6.12	0.83	40.4	-0.31	-0.09	-0.10
10385	SOL2003-06-18T06:26	W00 N28	0.31	0.89	0.54	56.2	0.26	0.03	0.02
10391	SOL2003-06-24T22:22	W10 N15	-0.31	-1.00	0.65	50.3	-0.30	-0.02	-0.02
10415	SOL2003-07-20T12:46	E21 N13	0.94	2.98	0.71	48.1	-0.19	0.06	0.06
10440	SOL2003-08-22T19:11	W05 S08	-1.88	-4.19	0.57	42.8	-0.17	-0.13	-0.10
10441	SOL2003-08-25T06:27	E02 N12	-0.63	-1.85	0.74	40.0	-0.16	-0.03	-0.03
10445	SOL2003-08-27T01:35	E20 N08	-0.63	-1.76	0.71	36.5	-0.26	-0.03	-0.03
10456	SOL2003-09-12T06:24	W37 S08	0.94	10.9	1.17	56.4	0.26	0.08	0.07
10488	SOL2003-10-29T15:59	W12 N07	0.31	22.7	3.60	55.2	-0.06	0.02	0.02
10495	SOL2003-11-01T09:35	E00 S22	-1.57	-8.82	0.81	62.8	-0.63	-0.13	-0.12
10547	SOL2004-02-01T19:11	W10 S10	-1.76	-1.98	0.52	36.4	-0.40	-0.07	-0.08
10565	SOL2004-02-26T12:51	W02 S04	0.63	6.43	0.96	67.5	0.46	0.07	0.05
10569	SOL2004-03-07T08:03	W03 S12	-2.45	-1.76	0.35	46.9	-0.10	-0.15	-0.14
10617	SOL2004-05-19T19:11	W15 S10	-0.31	-1.19	0.59	45.5	-0.05	-0.03	-0.02
10664	SOL2004-08-23T11:11	E04 S10	0.31	2.06	0.76	82.6	1.23	0.04	0.03
10692	SOL2004-10-27T01:39	W00 S18	-0.31	-0.51	0.39	75.7	-0.40	-0.03	-0.03
10747	SOL2005-04-05T01:39	W34 S07	-0.63	-4.02	0.71	58.7	-0.05	-0.08	-0.05
10837	SOL2005-12-20T19:12	W16 S10	-1.26	-8.96	0.89	61.4	-0.10	-0.11	-0.10
10879	SOL2006-05-03T12:47	E00 N16	-0.94	-0.58	0.31	34.6	-0.22	-0.06	-0.04
10900	SOL2006-07-19T01:36	W13 S04	0.63	1.51	0.52	57.3	0.57	0.06	0.04
10955	SOL2007-05-11T11:11	E01 S09	0.63	1.45	0.55	54.6	0.19	0.05	0.04
10971	SOL2007-09-29T12:51	W00 N02	0.63	0.10	0.19	29.4	0.27	0.03	0.02
10987	SOL2008-03-27T12:47	E01 S07	1.57	6.51	0.74	59.5	0.04	0.12	0.12
11007	SOL2008-11-02T19:15	W22 N36	-1.26	-1.20	0.34	45.0	-0.38	-0.11	-0.07
11010	SOL2009-01-12T07:59	W01 N20	-1.51	-0.82	0.30	43.0	-0.16	-0.09	-0.08
11024	SOL2009-07-07T06:24	W30 S25	-0.94	-8.31	0.79	73.3	-0.19	-0.13	-0.09
11027	SOL2009-09-25T12:47	W03 N23	-0.94	-0.82	0.33	60.6	-0.13	-0.07	-0.07
11043	SOL2010-02-02T19:15	W03 N25	1.57	0.96	0.26	47.8	0.54	0.14	0.09
11049	SOL2010-02-20T12:51	W32 S20	-0.31	-0.92	0.50	55.2	-0.09	-0.04	-0.02
11141	SOL2011-01-01T19:00	W20 N35	-0.94	-0.79	0.28	58.2	-0.25	-0.10	-0.07
11142	SOL2011-01-04T15:01	W00 S14	0.31	0.58	0.45	59.1	0.27	0.03	0.02

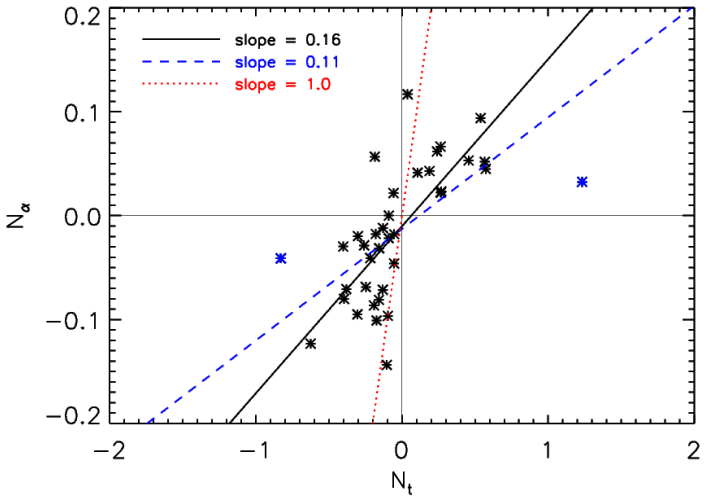

Figure 5. Number of turns [N_α] from Equation (8) *vs.* N_t from Poisson *et al.* (2015) for the ARs studied. The blue-dashed line corresponds to a linear regression of all the data. The blue asterisks mark the two most extreme cases that are likely responsible for the apparently small slope of the blue-dashed line. The black-continuous line represents a linear regression of the AR data indicated with black asterisks. The corresponding slopes are provided in the panel. The red-dotted line has a slope equal to unity and is included as a reference (see the discussion in Section 5).

are reasonable. A linear regression of the plot provides a slope close to 1 (0.82). Interestingly, if we use the definition of the number of turns provided by Pevtsov, Maleev, and Longcope (2003) (their Equation (1)) instead of our own expression from Equation (8), the obtained slope would be very close to 1, since this would imply a change of N_α by a factor 1.27. The above results imply that both definitions of the coronal number of turns, given by Equations (3) and (8), could be, in principle, alternatively used within the limitations of their estimations. However, the value of N_H depends on the size of the region used to compute Φ and H. As we discussed in Section 4.1, given the overestimation of H due to the requirements of the extrapolation procedure, the actual choice of the observational box for Φ and computational box for H calculations are rather arbitrary. A study of the effect of the selected boxes on the computation of N_H, for a small subset of the analyzed ARs, confirms this conclusion. For a subset of five ARs, a four times increase in the selected observational box size, keeping the computational box fixed, produces an average reduction to half in the value of N_H. It is worth remarking that this variation in N_H due to changes in the box size relates to the combined effect of the variation of H and Φ, since both are in general affected by the observational box size changes. Among the five studied ARs, in some cases the changes are mainly due to variations in Φ and in others due to changes in both H and Φ. Therefore, it is not easy to find a single explanation that applies to all studied cases. Since N_α, although depending on very strong approximations, does not have this kind of limitation, it appears to

be a more robust proxy for the number of turns. In what follows, we use N_α to compare with the number of turns obtained in Poisson *et al.* (2015).

The parameter N_t shown in Table 1 corresponds to $\bar{N}_{t,c}$ computed by Poisson *et al.* (2015). This is the number of turns inferred from the mean tongue angle (see Section 1) computed during the AR emergence. N_t is computed using an expression that assumes the emergence of a magnetic-flux rope with a half-torus shape (see Equation (6) of Poisson *et al.* (2015)). The subscript "c" stands for "corrected", because the computation includes a correction to account for the effect of the magnetic tongues on the AR tilt.

Figure 5 shows the relation between N_α and N_t. Although with an appreciable dispersion, the plot indicates a correlation between both parameters. The handedness of the twist, provided by the sign of N_α and N_t, is the same for most ARs. It is noteworthy that of the few exceptions, two correspond to ARs with small values of N_α and N_t (one of them has $N_\alpha = 0$), indicating that their field configuration is very close to potential. The remaining case (AR 10415) is the only one in the set with clearly different signs of N_α and N_t. Whether this difference is due to errors in the α determination or in the tongues procedure, we are not presently able to determine. Considering the tendency observed in the great majority of the cases, we conclude that the relation between N_α and N_t values is reasonable within the errors associated to the twist-determination procedure.

A linear regression that includes all the data (the blue-dashed line in Figure 5) indicates a slope of 0.11. This slope appears to be too small considering the distribution of the points. Indeed, the least-square fit is known to be strongly affected by outsider points located far away from the core of the distribution. Then, we include another regression, indicated with a black-continuous line, for which we removed the two extreme cases shown in blue. We also use a robust fit, which minimizes the total distance of the data points to the straight line (while the least-square fit minimizes the square of this distance). The results of the robust fit, with all data points, is close to the black line in Figure 5. This confirms the bias introduced by the outliers points in the lower slope found with the least-square fit (blue-dashed line).

To summarize, the previous results imply that N_t tends to be one order of magnitude larger than N_α, being on average, according to the slope of the black line, six times larger. We estimate that there are two main reasons for this, as follows.

In Poisson *et al.* (2015), N_t is assumed to be the total number of turns of a hypothetical half-torus flux rope whose top emerged. In contrast, N_α counts only the number of turns for the emerged part. This is likely to be the main reason why N_α and N_t differ on average by a factor of six. Moreover, the fact that the analyzed ARs correspond to flux ropes that have possibly emerged in different proportions might be one of the main factors behind the dispersion observed in the plot of Figure 5. There is also a dispersive effect due to the errors associated with the procedures to determine the different parameters.

Another possible source of dispersion could be the partial relaxation of twist due to the production of active phenomena during the analyzed evolution. While N_t is an average computed along the AR emergence phase, N_α is computed just

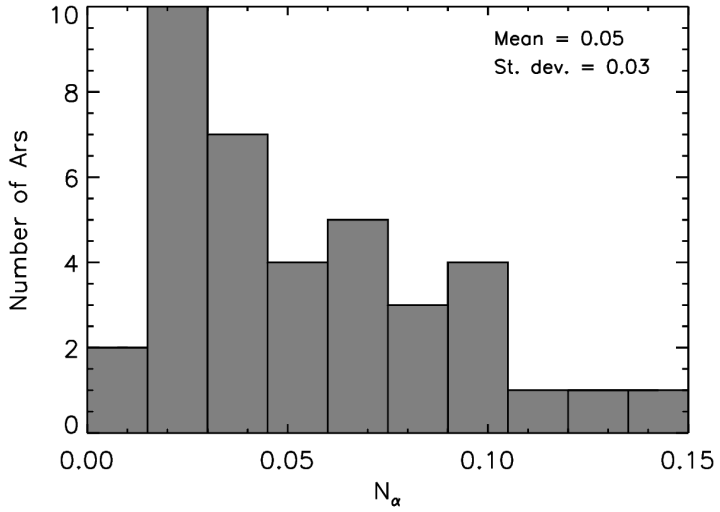

Figure 6. Histogram of N_α, obtained from Equation (8), for the ARs listed in Table 1. The mean and the standard deviation of the data are provided.

around the date of maximum flux emergence (see Section 3). Therefore, if the AR produced active events in the days or hours before the N_α computation, this parameter could be smaller than it had been if no activity were present. We analyzed this possibility by studying the relation between N_α and N_t in function of the total X-ray flux, measured by GOES, due to all of the active events produced by each AR during the analyzed periods. Although we did not find any correlation supporting this possibility, we cannot completely discard the hypothesis that this effect is partially present.

Comparing the statistical characteristics of both determinations (coronal and photospheric) of the number of turns, Figure 6 shows that N_α has a broad and asymmetric distribution for our AR set (a longer tail for larger values), which is similar to that of N_t shown in Figure 14 of Poisson *et al.* (2015). The distribution of N_α has a mean of 0.05 and a standard deviation of approximately 60 % of its mean value, which is again similar to what is found for N_t.

To conclude, the results in Figures 5 and 6 indicate a direct relation between the twist inferred at the photosphere and the corona and confirm the validity of the magnetic-tongue method analyzed in Poisson *et al.* (2015) to have an early proxy of an AR twist.

6. Conclusions

In this work we analyze the magnetic twist of ARs, which we convert to the number of turns, inferred from LFFF models of their coronal structures observed in SOHO/EIT and SDO/AIA images. The main motivation is to compare our results with those obtained by Poisson *et al.* (2015), who studied the same set of

ARs and determined the number of turns of bipolar ARs, considering the effect of magnetic tongues in observed line-of-sight photospheric magnetograms. We found a reasonable consistency between the results from both determinations, as follows.

We analyze two alternative ways to obtain the number of turns from the LFFF models of the AR coronal field. In the first one, we relate the magnetic helicity obtained from the models with the number of turns [$N_{\rm H}$] of an equivalent twisted flux-tube with the same magnetic helicity (see Equation (3)). In the second one, we directly relate the force-free parameter α from the models with the number of turns [N_α] derived for a classical flux-rope configuration: the Lundquist constant-α model. In Appendix A, we also analyze the Gold–Hoyle constant-twist case. We show that, under reasonable approximations, α can be related to the number of turns of an equivalent flux-rope (see Equations (8) and (14)). The comparison between $N_{\rm H}$ and N_α for the set of analyzed ARs indicates that both alternative determinations give close results.

Finally, we compare N_α with the parameter $N_{\rm t}$ given by Poisson *et al.* (2015). The plot of N_α *vs.* $N_{\rm t}$ shows that both parameters have the same sign for almost all ARs. The distribution of points in the plot indicates a trend for which $N_\alpha \approx 0.16\, N_{\rm t}$. In Section 5, we conclude that the difference between both parameters is mainly due to the definition of $N_{\rm t}$ as the total number of turns of a half-torus flux rope that has partially emerged and the definition of N_α (alternatively, $N_{\rm H}$) that corresponds only to the emerged part (*i.e.* the LFFF model). The dispersion of $N_\alpha/N_{\rm t}$ values could be due to the fact that different ARs are produced by flux ropes that have emerged in different degrees (fractions of the sub-photospheric flux-rope) and/or have had a different number of active events (in particular, in terms of CMEs).

Appendix

A. Force-Free Flux-Rope with Constant Twist: the Gold-Hoyle Model

Let us consider the case of a flux tube with uniform twist, *i.e.* with b constant in Equation (5). This corresponds to the so-called Gold–Hoyle flux-rope model. In this model α is a function of r. The magnetic field of the rope in cylindrical coordinates is $\boldsymbol{B} = (0, B_\theta(r), B_z(r))$. Writing the force-free Equation (1) in the form:

$$(\nabla \times \boldsymbol{B}) \times \boldsymbol{B} = 0, \tag{9}$$

and using Equation (5) one can solve the components of the field obtaining:

$$B_z = \frac{B_0}{(1 + b^2 r^2)}, B_\theta = \frac{B_0\ r\ b}{(1 + b^2 r^2)}. \tag{10}$$

Replacing these expressions in the force-free equation written in its usual form: $\nabla \times \boldsymbol{B} = \alpha \boldsymbol{B}$, and solving for α in any of the two components of the equation

gives:

$$\alpha(r) = \frac{2b}{(1 + b^2 r^2)}. \tag{11}$$

This expression provides the dependence of α in function of r. We define an average α along the flux-tube radius $[a]$ as:

$$\bar{\alpha} = \frac{1}{a} \int_0^a \frac{2b \, \mathrm{d}r}{(1 + b^2 r^2)} = \frac{2}{a} \arctan(ab). \tag{12}$$

Solving this expression for b and using Equation (7), we find

$$N_{\bar{\alpha}} = \frac{L}{2\pi a} \tan\left(\frac{\bar{\alpha} a}{2}\right). \tag{13}$$

Considering that in general $\bar{\alpha}a$ is small, $\tan\left(\frac{\bar{\alpha}a}{2}\right) \approx \frac{\bar{\alpha}a}{2}$, and then using $L = \pi D/2$ for the length of half a torus of diameter D:

$$N_{\bar{\alpha}} \approx \frac{\bar{\alpha} D}{8}. \tag{14}$$

Replacing $\bar{\alpha}$ by α we recover the result of Equation (8). This demonstrates that, considering reasonable approximations, the two most usual flux-rope descriptions provide similar relations between α and the number of turns, even though they are different in nature (*i.e.* α is a constant for the Lundquist solution and it depends on r for the Gold–Hoyle model).

Acknowledgments The authors sincerely thank the anonymous referee for his/her useful comments and suggestions. MLF and CHM are members of the Carrera del Investigador Científico of the Consejo Nacional de Investigaciones Científicas y Técnicas (CONICET) of Argentina. MP is a CONICET Fellow. MP, MLF and CHM acknowledge financial support from the Argentinean grants PICT 2012-0973 (ANPCyT), UBACyT 20020130100321 and PIP 2012-01-403 (CONICET).

Disclosure of Potential Conflicts of Interest

The authors declare that they have no conflicts of interest.

References

Alissandrakis, C.E.: 1981, On the computation of constant alpha force-free magnetic field. *Astron. Astrophys.* **100**, 197. ADS.

Berger, M.A.: 1984, Rigorous new limits on magnetic helicity dissipation in the solar corona. *Geophys. Astrophys. Fluid. Dyn.* **30**, 79. DOI. ADS.

Berger, M.A.: 1985, Structure and stability of constant-alpha force-free fields. *Astrophys. J. Suppl.* **59**, 433. DOI. ADS.

Berger, M.A.: 1999, Introduction to magnetic helicity. *Plasma Physics and Controlled Fusion* **41**, 167. DOI. ADS.

Burnette, A.B., Canfield, R.C., Pevtsov, A.A.: 2004, Photospheric and Coronal Currents in Solar Active Regions. *Astrophys. J.* **606**, 565. DOI.

Delaboudinière, J.-P., Artzner, G.E., Brunaud, J., Gabriel, A.H., Hochedez, J.F., Millier, F., *et al.*: 1995, EIT: extreme-ultraviolet imaging telescope for the SOHO mission. *Solar Phys.* **162**, 291. DOI. ADS.

Démoulin, P., Pariat, E.: 2009, Modelling and observations of photospheric magnetic helicity. *Adv. Space Res.* **43**, 1013. DOI. ADS.

Démoulin, P., Mandrini, C.H., van Driel-Gesztelyi, L., Thompson, B.J., Plunkett, S., Kovári, Z., Aulanier, G., Young, A.: 2002, What is the source of the magnetic helicity shed by CMEs? The long-term helicity budget of AR 7978. *Astron. Astrophys.* **382**, 650. DOI. ADS.

Emonet, T., Moreno-Insertis, F.: 1998, The Physics of Twisted Magnetic Tubes Rising in a Stratified Medium: Two-dimensional Results. *Astrophys. J.* **492**, 804. DOI. ADS.

Fan, Y.: 2001, Nonlinear Growth of the Three-dimensional Undular Instability of a Horizontal Magnetic Layer and the Formation of Arching Flux Tubes. *Astrophys. J.* **546**, 509. DOI. ADS.

Fan, Y.: 2009, Magnetic Fields in the Solar Convection Zone. *Living Rev. Solar Phys.* **6**, 4. DOI. ADS.

Gosain, S., Démoulin, P., López Fuentes, M.: 2014, Distribution of Electric Currents in Sunspots from Photosphere to Corona. *Astrophys. J.* **793**, 15. DOI. ADS.

Green, L.M., López fuentes, M.C., Mandrini, C.H., Démoulin, P., Van Driel-Gesztelyi, L., Culhane, J.L.: 2002, The Magnetic Helicity Budget of a cme-Prolific Active Region. *Solar Phys.* **208**, 43. DOI. ADS.

Holder, Z.A., Canfield, R.C., McMullen, R.A., Nandy, D., Howard, R.F., Pevtsov, A.A.: 2004, On the Tilt and Twist of Solar Active Regions. *Astrophys. J.* **611**, 1149. DOI. ADS.

Hood, A.W., Archontis, V., MacTaggart, D.: 2012, 3D MHD Flux Emergence Experiments: Idealised Models and Coronal Interactions. *Solar Phys.* **278**, 3. DOI. ADS.

Lemen, J.R., Title, A.M., Akin, D.J., Boerner, P.F., Chou, C., Drake, J.F., *et al.*: 2012, The Atmospheric Imaging Assembly (AIA) on the Solar Dynamics Observatory (SDO). *Solar Phys.* **275**, 17. DOI. ADS.

Longcope, D.W., Welsch, B.T.: 2000, A Model for the Emergence of a Twisted Magnetic Flux Tube. *Astrophys. J.* **545**, 1089. DOI. ADS.

López Fuentes, M.C., Klimchuk, J.A., Démoulin, P.: 2006, The Magnetic Structure of Coronal Loops Observed by TRACE. *Astrophys. J.* **639**, 459. DOI. ADS.

López Fuentes, M.C., Demoulin, P., Mandrini, C.H., van Driel-Gesztelyi, L.: 2000, The Counterkink Rotation of a Non-Hale Active Region. *Astrophys. J.* **544**, 540. DOI. ADS.

López Fuentes, M.C., Démoulin, P., Mandrini, C.H., Pevtsov, A.A., van Driel-Gesztelyi, L.: 2003, Magnetic twist and writhe of active regions. On the origin of deformed flux tubes. *Astron. Astrophys.* **397**, 305. DOI. ADS.

Luoni, M.L., Démoulin, P., Mandrini, C.H., van Driel-Gesztelyi, L.: 2011, Twisted Flux Tube Emergence Evidenced in Longitudinal Magnetograms: Magnetic Tongues. *Solar Phys.* **270**, 45. DOI. ADS.

Mandrini, C.H., Démoulin, P., van Driel-Gesztelyi, L., Green, L., López Fuentes, M.C.: 2004, Magnetic helicity budget of solar-active regions from the photosphere to magnetic clouds. *Astrophys. Space Sci.* **290**, 319. DOI. ADS.

Mandrini, C.H., Pohjolainen, S., Dasso, S., Green, L.M., Démoulin, P., van Driel-Gesztelyi, L., *et al.*: 2005, Interplanetary flux rope ejected from an X-ray bright point. The smallest magnetic cloud source-region ever observed. *Astron. Astrophys.* **434**, 725. DOI. ADS.

Pariat, E., Aulanier, G., Schmieder, B., Georgoulis, M.K., Rust, D.M., Bernasconi, P.N.: 2004, Resistive Emergence of Undulatory Flux Tubes. *Astrophys. J.* **614**, 1099. DOI. ADS.

Pevtsov, A.A., Maleev, V.M., Longcope, D.W.: 2003, Helicity Evolution in Emerging Active Regions. *Astrophys. J.* **593**, 1217. DOI. ADS.

Pevtsov, A.A., Berger, M.A., Nindos, A., Norton, A.A., van Driel-Gesztelyi, L.: 2014, Magnetic Helicity, Tilt, and Twist. *Space Sci. Rev.* **186**, 285. DOI. ADS.

Poisson, M., Mandrini, C.H., Démoulin, P., López Fuentes, M.: 2015, Evidence of Twisted Flux-Tube Emergence in Active Regions. *Solar Phys.* **290**, 727. DOI. ADS.

Scherrer, P.H., Bogart, R.S., Bush, R.I., Hoeksema, J.T., Kosovichev, A.G., Schou, J., *et al.*: 1995, The Solar Oscillations Investigation - Michelson Doppler Imager. *Solar Phys.* **162**, 129. DOI. ADS.

Scherrer, P.H., Schou, J., Bush, R.I., Kosovichev, A.G., Bogart, R.S., Hoeksema, J.T., *et al.*: 2012, The Helioseismic and Magnetic Imager (HMI) Investigation for the Solar Dynamics Observatory (SDO). *Solar Phys.* **275**, 207. DOI. ADS.

Sturrock, P.A.: 1994, *Plasma Physics, An Introduction to the Theory of Astrophysical, Geophysical and Laboratory Plasmas*, 1994, Cambridge University Press, Cambridge, UK, ??? ADS.

Szajko, N.S., Cristiani, G., Mandrini, C.H., Dal Lago, A.: 2013, Very intense geomagnetic storms and their relation to interplanetary and solar active phenomena. *Adv. Space Res.* **51**, 1842. DOI. ADS.

Tziotziou, K., Georgoulis, M.K., Raouafi, N.-E.: 2012, The Magnetic Energy-Helicity Diagram of Solar Active Regions. *Astrophys. J. Lett.* **759**, L4. DOI. ADS.

Valori, G., Green, L.M., Démoulin, P., Vargas Domínguez, S., van Driel-Gesztelyi, L., Wallace, A., Baker, D., Fuhrmann, M.: 2012, Nonlinear Force-Free Extrapolation of Emerging Flux with a Global Twist and Serpentine Fine Structures. *Solar Phys.* **278**, 73. DOI. ADS.

Vargas Domínguez, S., van Driel-Gesztelyi, L., Bellot Rubio, L.R.: 2012, Granular-Scale Elementary Flux Emergence Episodes in a Solar Active Region. *Solar Phys.* **278**, 99. DOI. ADS.

Yang, S., Zhang, H., Büchner, J.: 2009, Magnetic helicity accumulation and tilt angle evolution of newly emerging active regions. *Astron. Astrophys.* **502**, 333. DOI. ADS.